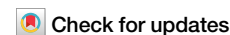




# Stratospheric transport and tropospheric sink of solar geoengineering aerosol: a Lagrangian analysis



Hongwei Sun<sup>1,2</sup>✉, Stephen Bourguet<sup>3</sup>, Lan Luan<sup>4</sup> & David Keith<sup>1,2</sup>

Stratospheric aerosol injection (SAI) aims to reflect solar radiation by increasing the stratospheric aerosol burden. To understand how the background circulation influences stratospheric transport of injected particles, we use a Lagrangian trajectory model (lacking numerical diffusion) to quantify particles' number, flux, lifetime, and tropospheric sinks from a SAI injection strategy under present-day conditions. While particles are being injected, stratospheric particle number increases until reaching a steady-state. During the steady-state, the time series of particle number shows a dominant period of ~2 years (rather than a 1-year cycle), suggesting modulation by the quasi-biannual oscillation. More than half of particles, injected in the tropical lower stratosphere (15° S to 15° N, 65 hPa), undergo quasi-horizontal transport to the midlatitude. We find a zonal asymmetry of particles' tropospheric sinks that are co-located with tropopause folding beneath the midlatitude jet stream, which can help predict tropospheric impacts of SAI (e.g., cirrus cloud thinning).

Given the anthropogenically forced changes to Earth's climate and the persistent difficulties in controlling greenhouse gas (GHG) emissions, solar geoengineering has been considered a method to reduce global warming, which should be combined with GHG emission reductions<sup>1,2</sup>. Stratospheric aerosol injection (SAI) is one of the widely studied methods of solar geoengineering<sup>3–6</sup>, which aims to reflect solar radiation by injecting aerosols or their precursors into the stratosphere. Volcanic eruptions can be considered natural analogs for SAI<sup>7–9</sup>.

It is important to understand how injected particles would be transported in the stratosphere, which can help us better estimate the climatic impacts of SAI<sup>10–15</sup> and guide the design of injection strategies<sup>16–20</sup>. For example, based on the poleward transport of the stratospheric Brewer–Dobson circulation (BDC), a combination of injections at multiple latitudes can achieve different spatial patterns of AOD to tailor the climatic impacts of SAI<sup>21</sup>. Additionally, particles injected at different longitudes in the tropical lower stratosphere can have different poleward transport pathways, resulting in different particle lifetimes in the stratosphere<sup>22</sup>.

The transport of injected particles in the stratosphere can be influenced by many factors, such as aerosol microphysical growth<sup>23,24</sup> and the background circulation of the atmosphere<sup>25,26</sup>. This study uses a Lagrangian trajectory model driven by reanalysis data to simulate the stratospheric transport of passive particles (neglecting aerosol's microphysical growth or radiative effects) from a SAI injection strategy, to focus on how the

background circulation and its variability influence the transport of injected particles in the stratosphere.

Lagrangian trajectory models have high computational efficiency and lack numerical diffusion, which makes them good at tracking the location of individual particles in the stratosphere. This can help us better understand both particle-scale transport and the statistical properties of large injections in the stratosphere for SAI. Even though Lagrangian trajectory models have been widely used in simulating the transport of water vapor, ozone, and volcanic particles<sup>27–29</sup>, there are limited SAI studies using this Lagrangian method<sup>22,30</sup>.

Therefore, we apply this type of model to the SAI research field, aiming to gain accurate and quantitative evaluations of the particle transport (including particle number, flux, lifetime, and tropospheric sinks) in the stratosphere, and explore how features of the background circulation (e.g., quasi-biennial oscillation (QBO), tropopause folding) influence particle transport. Our results from the Lagrangian method can be complementary to previous SAI studies using global climate models (GCMs). Comparisons between the Lagrangian trajectory model and the global climate models are provided in the “Discussion” section, which indicates the scope of applications of the two different model types. Moreover, as previous studies have shown that surface air pollutants (e.g., ozone) can be influenced by stratospheric intrusion<sup>31,32</sup>, this Lagrangian method can identify tropospheric sinks of injected particles (where particles cross the tropopause from the

<sup>1</sup>School of Engineering and Applied Sciences, Harvard University, Cambridge, MA, USA. <sup>2</sup>Department of the Geophysical Sciences, The University of Chicago, Chicago, IL, USA. <sup>3</sup>Department of Earth and Planetary Sciences, Harvard University, Cambridge, MA, USA. <sup>4</sup>Department of Earth and Atmospheric Sciences, Indiana University Bloomington, Bloomington, IN, USA. ✉e-mail: [hongwei8@uw.edu](mailto:hongwei8@uw.edu)

stratosphere to the troposphere), which can help us better estimate SAI's influences on the troposphere (e.g., cirrus cloud thinning, local air pollution).

## Results

### Number of particles in the stratosphere

In this study, we adopt a Lagrangian trajectory model (i.e., LAGRANTO), modified to include particle sedimentation<sup>33,34</sup>, to simulate particle transport (driven by ERA5 reanalysis wind field data) under a SAI injection strategy that injects passive particles once every 3 days at 19 km (65 hPa) within the tropical (15° S to 15° N) stratosphere for 10 years (2000.01–2010.01). This is described in detail in the “Methods” section (section “LAGRANTO model settings”).

Figure 1 shows the time series of the total particle number in the stratosphere, which can be divided into three stages. The first period is the increasing stage (2000.01–2005.01): the number of particles in the stratosphere increases due to continuous injection. With the increase of the stratospheric particle load, the tropospheric sink rate (i.e., the downward stratosphere-to-troposphere particle flux, defined in section “Calculation of downward stratosphere-to-troposphere particle number flux (ST-flux)”) increases until reaching the injection rate, which marks the transition to the steady-state stage (2005.01–2010.01). There is still a slight increase in particle numbers in the stratosphere during this stage (less than 1.5% increase per year), but the steady-state properties of transport dominate over this secular change. When we stop injection on Jan 1, 2010, the third stage (decreasing stage) begins, as there are no new particles injected into the stratosphere and particles in the stratosphere would finally reach the tropopause and exit the stratosphere. The decreasing trend can be approximately represented by an exponential decay function  $N(t) = N(0) \cdot e^{-t/\tau}$ , where  $t$  is the number of days after injection stops on Jan 1, 2010,  $N$  is the number of particles in the stratosphere ( $N(0) = 60,462$ ), and  $\tau$  is the exponential time constant (i.e., 576 days here). These three stages also show up in the time series of particles injected at different altitudes (18, 19, 20, and 22 km), as shown in Supplementary Fig. 3.

By applying the Morlet wavelet transform<sup>35,36</sup> to the time series of the stratospheric particle number during the steady-state stage, we find there are 1-year (seasonal cycle) and 2-year periods. Interestingly, the 2-year period is dominant (Fig. 2a). This roughly aligns with the QBO, as shown in Fig. 2b. The QBO is a dynamic mode of variability in the tropical stratosphere with a period varying between ~2 and 3 years<sup>37</sup>. Thus, this 2-year period may indicate that the QBO could modulate particle number in the stratosphere, which is consistent with previous GCM model results showing that QBO can modulate stratospheric sulfate lifetime<sup>26</sup>. Since the QBO cannot influence the source of particles in the stratosphere (i.e., a constant injection rate), it may influence the sink of stratosphere particles to modulate particle number in the stratosphere.

We calculate the downward stratosphere-to-troposphere particle number flux (hereafter, ST-flux), which is defined as the number of particles crossing the tropopause from the stratosphere to the troposphere in section “Calculation of downward stratosphere-to-troposphere particle number flux (ST-flux),” to identify the tropospheric sink of injected particles. The ST-flux can be considered as the rate at which stratospheric particle number changes with time (i.e., ST-flux is the derivative of stratospheric particle number with respect to time). For example, the maximum ST-flux can cause the largest decreasing rate of stratospheric particle number (see black and red lines in Supplementary Fig. 4).

Figure 2b shows a high correlation with a time lag of 7 months (the lagged correlation coefficient of 0.8) between the time series of ST-flux and the QBO index (i.e., 50 hPa monthly mean zonal wind derived from daily Singapore observation site), indicating a larger ST-flux following the QBO West phase (positive QBO index values) and a smaller ST-flux following the QBO East phase (negative QBO index values). This lagged correlation may indicate the time for the QBO's influence to transport from the tropics (where QBO originates) to the midlatitude (where most ST-flux happens, as shown in Fig. 5), which means the QBO index can be a useful predictor to help us estimate the time variation of particle number in the stratosphere.

Previous studies have shown that the QBO can modulate the stratosphere-troposphere exchange<sup>38,39</sup> which can then influence the total number of particles in the stratosphere. In the tropics and subtropics, the

**Fig. 1** | Time series of the number of particles (black line) in the stratosphere, with three stages divided by the red dashed lines.

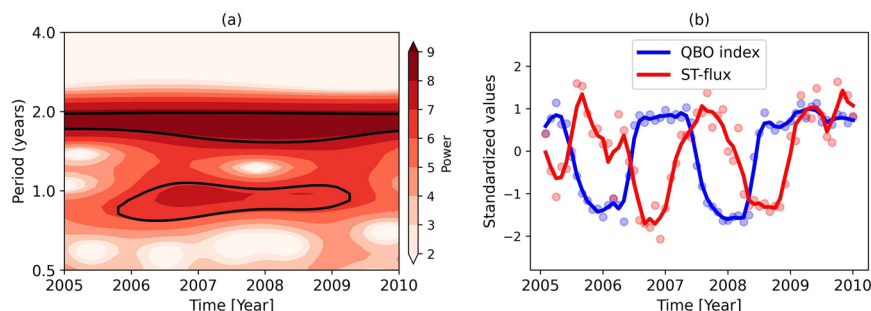
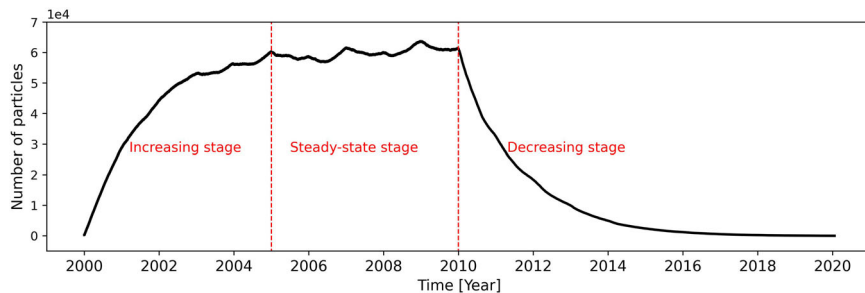


**Fig. 2** | Relationship between QBO and particle number in the stratosphere. **a** Wavelet power spectrum of the time series of particle number in the stratosphere based on the Morlet wavelet transform<sup>35</sup>. The thick black contour encloses regions of greater than the 95% confidence level. **b** Standardized time series of QBO index (i.e.,

50 hPa monthly mean zonal wind derived from daily Singapore observation site) and standardized time series of stratosphere-to-troposphere number flux (ST-flux) (removed linear trend and seasonal cycle). A 3-month moving average (line) is applied to the monthly data (dots).

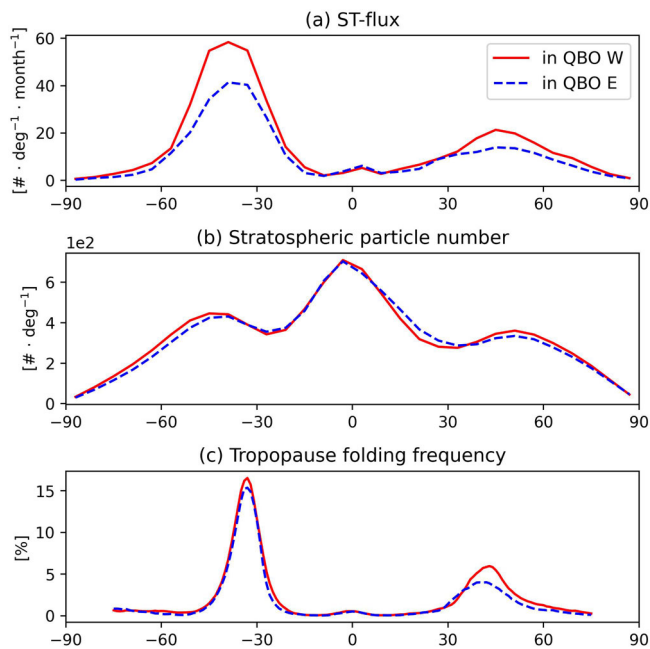


**Fig. 3 | QBO’s influences on ST-flux, stratospheric particle number, and tropopause folding frequency.** Latitudinal distribution of **a** ST-flux (zonally integrated) with a unit of particles per degree (latitude) per month, **b** stratospheric column concentration of particle number (zonally integrated) with a unit of particles per degree (latitude), and **c** tropopause folding frequency (zonally averaged) (unit: %) during QBO West (red line) and East (blue line) phases.

QBO can induce a secondary meridional circulation that influences the BDC and stratospheric transport<sup>40,41</sup>. The QBO can also exert influences on the stratospheric polar vortex by affecting the planetary wave propagation via the Holton–Tan mechanism<sup>42–44</sup>.

For the cluster analysis shown in Fig. 3, we define the QBO West (East) phase as the months with a positive (negative) QBO index (the blue line in Fig. 2b). To eliminate influences from the seasonal cycle, we choose January, February, and March in 2005, 2007, and 2009 to represent the QBO West phase, while the QBO East phase is represented by the same months in 2006 and 2008. Besides the high correlation coefficient (lagged) between ST-flux and QBO index (Fig. 2b), Fig. 3a shows that ST-flux, mainly happening in the midlatitudes, is larger in the QBO West phase than in the East phase (note: the time lag of 7 months is considered in the cluster analysis), which is consistent with previous studies<sup>26</sup>. Here, we conclude that the QBO modulates the ST-flux (or total number of particles in the stratosphere) in two ways:

- Firstly, the QBO can cause a secondary meridional circulation, which can change the particle number distribution, especially the meridional distribution. Figure 3b shows that there are fewer (more) particles in the tropics (midlatitude) in the QBO West phase than in the East phase, indicating that the secondary meridional circulation in the QBO West phase (compared to the East phase) could transport more particles from tropics to the midlatitudes<sup>45</sup>. This higher particle concentration in the midlatitude in the QBO West phase (Fig. 3b), especially near the midlatitude tropopause (Supplementary Fig. 5)<sup>46</sup>, would result in a larger ST-flux in the midlatitude (Fig. 3a).
- Secondly, Fig. 3c shows that the frequency of tropopause folding (also known as double tropopause, which can be accessed from <https://datapub.fz-juelich.de/slcs/tropopause/><sup>47</sup>) is larger in the QBO West phase than in the East phase. A larger tropopause folding frequency allows more particles in the stratosphere to be irreversibly (due to the particle sedimentation and tropospheric wet deposition, see section “Calculation of downward stratosphere-to-troposphere particle number flux (ST-flux)”) transported across the tropopause into the troposphere, resulting in a larger ST-flux (Fig. 5). This is consistent

with previous studies<sup>48–51</sup> that explain how a QBO signal can extend from the tropics to the midlatitude (e.g., caused by the secondary meridional circulation<sup>52</sup>), which then influences the midlatitude jet stream and tropopause folding (tropopause folding often happens beneath the jet stream).

In summary, the variability of stratospheric particle number during steady-state is dominated by the ST-flux, which is influenced by two factors including particle concentration distribution and tropopause folding. The QBO can influence these two factors (Fig. 3b, c) to modulate the ST-flux (or total number of particles in the stratosphere) of particles initially injected in the tropical stratosphere. It is worth noting that the first mechanism’s influence on ST-flux could decrease when we choose to inject particles at a higher latitude (e.g., polar regions). However, the second mechanism would keep influencing the ST-flux even for a high-latitude injection. For particles injected at a higher latitude, there may be other ways for QBO to modulate the ST-flux (e.g., through the Holton–Tan mechanism).

### Particle transport in the stratosphere

Figure 4a shows the steady-state (2005.01–2010.01) spatial distribution of particle number concentration (concentration  $C = \frac{N}{D_y \cdot D_z}$ , where  $N$  is the zonal-integration of particle number over the Lat-Alt area  $D_y \cdot D_z$ ). The spatial distribution, with high concentrations in the tropical and lower stratosphere, is consistent with previous GCM results of SAI<sup>53,54</sup>. The highest concentration center is located above the injection location (yellow dots in Fig. 4a) due to the upwelling flow of the BDC in the tropical pipe<sup>53</sup>.

To further analyze particle transport in the stratosphere, we separate the stratosphere into several regions and calculate the steady-state (2005.01–2010.01) particle number ( $N$ , red values in Fig. 4b) and particle lifetime ( $L$ , purple values in Fig. 4b) in these regions and the particle number flux ( $F$ , blue values in Fig. 4b) between them. In the tropics, the upper and lower stratosphere are separated at 50 hPa, which allows us to separate the influences from deep and shallow branches of the BDC. Taking the particle sedimentation into consideration, we set the separation level (i.e., 50 hPa) lower than previous studies (e.g., 30 hPa<sup>55</sup>).

For a scaled injection rate of 100 particles per year in the tropical lower stratosphere (65 hPa), there are three pathways for injected particles to be transported. The first pathway is the downward transport (caused by particle sedimentation) from the stratosphere to the troposphere: 20% of injected particles directly move downward and cross the tropopause within the tropics. The second pathway is quasi-horizontal tropics-to-midlatitude (TM) transport (driven by the residual transport within the shallow branch of the BDC as well as isentropic mixing), which transports more than half of injected particles (56%) from the tropics to the midlatitudes. The third pathway is upward transport (driven by the tropical upwelling flow of the BDC), which lofts 24% of injected particles into the tropical upper stratosphere and then to the midlatitudes following the deep branch of the BDC. Even though the tropical region has the largest number of particles ( $48 + 44 = 92$ , from Fig. 4b), the majority (67%) of injected particles in the stratosphere cross the tropopause (i.e., tropospheric sink) in the midlatitude. The tropospheric sink will be discussed further in section “Tropospheric sink of injected particles”.

Based on the particle number ( $N$ ) and number flux ( $F$ ) during steady-state, we can calculate the particle lifetime ( $L = \frac{N}{F}$ ), which is similar to the age of air<sup>56,57</sup>, in different regions. Injected particles have a very short lifetime (0.4 years) in the tropical lower stratosphere due to the region’s proximity to the tropopause and the speed of the three transport pathways mentioned above. However, particles in the tropical upper stratosphere have a longer lifetime of 2.0 years, and particles in the midlatitude stratosphere have a lifetime of 0.8 years. If particles reach the polar stratosphere, they can have a long average lifetime of 2.3 years in this region due to a small tropospheric sink in the polar region.

### Tropospheric sink of injected particles

For SAI, the transport of injected particles in the stratosphere starts at the initial injection locations and ends at tropospheric sinks where particles

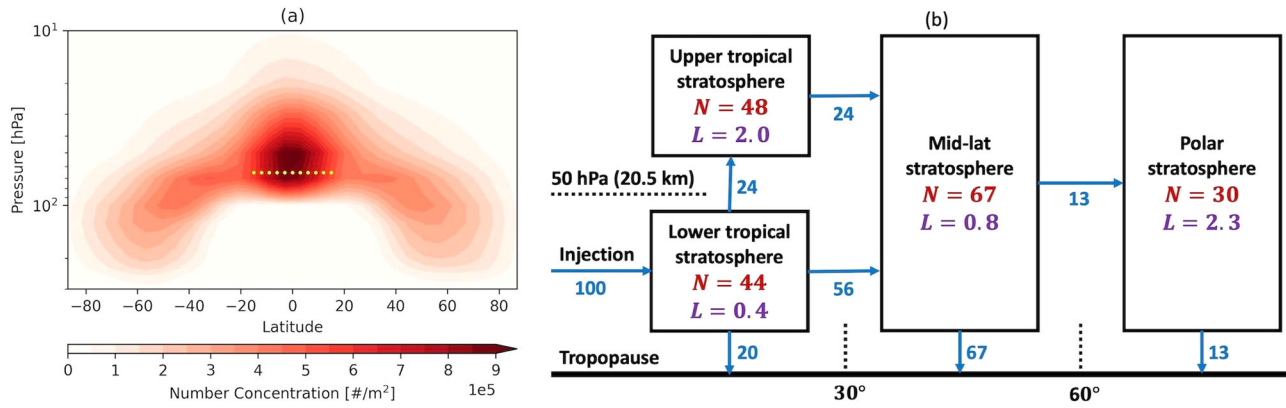


**Fig. 4 | Evaluations of particle distribution and transport in the stratosphere.** **a** Spatial distribution (latitude vs. altitude) of zonally integrated particle number concentration (with a unit of particles per square meter). **b** Particle number  $N$  (red values with the unit of particles), number flux  $F$  (blue values with a unit of particles

per year), and lifetime  $L$  (purple values with a unit of years) in or between different regions (black boxes) during the steady-state stage (2005.01–2010.01). The injection rate is scaled to 100 particles per year and all other values are scaled correspondingly.

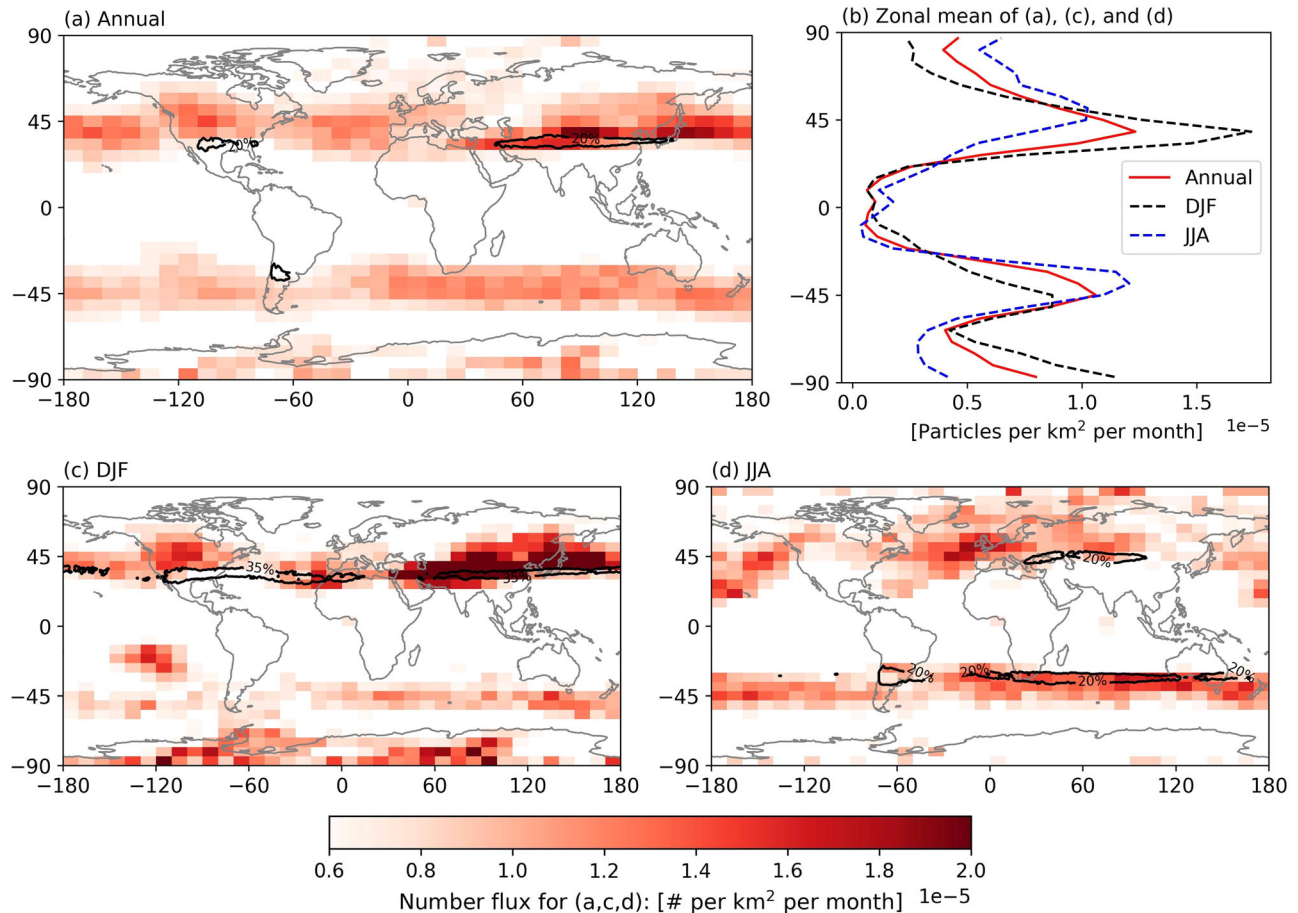


**Fig. 5 | Tropospheric sink of injected particles.** **a** Annual mean downward ST-flux (unit: particles per km<sup>2</sup> per month, shaded in red) and annual mean tropopause folding frequency (solid black contour lines marked with 20% or 35%) during the

steady-state stage. **b** Zonal mean of ST-flux from (a, c, d). **c, d** ST-flux and tropopause folding frequency in DJF and JJA, respectively.

cross the tropopause. Following previous studies<sup>22,47</sup>, we define the tropopause height as the lower of the following two heights: the thermal lapse rate tropopause<sup>58</sup> and the dynamical tropopause (based on thresholds of 3.5 potential vorticity units in the extra-tropics and 380 K of potential temperature in the tropics). Unlike initial injection locations that have been well studied for SAI<sup>22,53,59–61</sup>, limited studies<sup>62–64</sup> have considered the deposition of injected particles for SAI, such as evaluating the surface sulfate deposition

and its impacts on the ecosystem based on the simulation of a sulfate geoengineering scenario<sup>63</sup>. This study analyzes particles’ tropospheric sink (Fig. 5), which can help us identify places where injected particles are most likely to impact the upper troposphere (e.g. cirrus cloud thinning caused by SAI)<sup>65,66</sup> and surface (e.g. local air pollution caused by SAI<sup>67</sup>).

Figure 5 shows the ST-flux (see “Methods” section for details). Consistent with previous studies<sup>26,68</sup>, most particles cross the tropopause in the

midlatitudes. Figure 5b shows the seasonal cycle of ST-flux, with a larger ST-flux in the winter hemisphere (i.e., northern hemisphere in DJF or southern hemisphere in JJA) than in the summer hemisphere (i.e., southern hemisphere in DJF and northern hemisphere in JJA). Inside one hemisphere, there is leverage between midlatitude ST-flux and polar ST-flux, which means a stronger (weaker) midlatitude ST-flux would be paired with a weaker (stronger) polar ST-flux. This is because a stronger (weaker) midlatitude ST-flux could let more (fewer) particles exit the stratosphere in the midlatitude, so there will be fewer (more) particles entering the polar region, which can result in a weaker (stronger) polar ST-flux.

From Fig. 5a, we note a zonal asymmetry in tropospheric sinks, such as a larger ST-flux over Asia than elsewhere at the same latitude. Seasonally (Fig. 5c, d), there is a dominant tropospheric sink (with large ST-flux) over Asia in DJF, while in JJA, a dominant tropospheric sink is over Australia. Figure 5c, d show that the dominant tropospheric sinks (shaded in red) are located near the local maxima in the frequency of tropopause folding (contour lines in black), which often happens beneath the subtropical jet stream. This is likely a connection between tropopause folding and the transport of air mass (including particles) from the stratosphere into the troposphere<sup>69</sup>, resulting in the overlap between dominant tropospheric sinks and tropopause folding.

Though the spatial pattern (large ST-flux in midlatitudes) and seasonal cycle (large ST-flux in the winter hemisphere) of ST-flux in this study is consistent with the general pattern characterizing stratosphere-to-troposphere exchange<sup>70-72</sup>, the ST-flux derived from the injected particles, compared to the ST-flux derived from massless gases (e.g., air, ozone), shows discrepancies (specialties) in two ways:

- We consider the injected particle as a mass point with settling speed (i.e., sedimentation), which is different from the massless gases used in previous studies<sup>68,73,74</sup>. Compared to the massless gases, injected particles have a larger downward transport (due to the sedimentation process), which causes a shorter stratospheric lifetime and makes the ST-flux closer to the tropical injection locations. For example, the ST-flux derived from particles has a maximum over Asia (around 40° N) in DJF (Fig. 5c), where tropopause folding often happens beneath the midlatitude jet stream. While the ST-flux derived from air mass has a maximum over the North Atlantic (around 60° N)<sup>74</sup> where baroclinic disturbances in storm tracks can even transport stratospheric air into the marine boundary layer<sup>68</sup>.
- The ST-flux also highly depends on the concentration distribution. The particle concentration distribution, based on a tropical injection strategy, is different from the concentration distribution of air or ozone. Thus, the discrepancies in the concentration distribution of different species can introduce bias for the ST-flux estimation. For example, the ST-flux derived from ozone shows a peak along the Equator over the

Indian Ocean in JJA because of high ozone concentrations at the tropical tropopause<sup>75</sup>, which is different from the ST-flux derived from injected particles (Fig. 5d) or air.

## Discussion

This study quantifies the particle number, flux, lifetime, and tropospheric sinks for injected particles from a SAI injection strategy under present-day conditions, which can offer a better understanding of the whole life cycle of injected particles in the stratosphere. We explore the physical mechanisms of how the background circulation influences particle transport to explain a dominant 2-year period of particle number in the stratosphere and the zonal asymmetry of tropospheric sinks of injected particles. The former (the 2-year period) is likely a result of transport variability associated with the QBO (Figs. 2 and 3), while the latter (the tropospheric sink) is influenced by tropopause folding beneath the midlatitude jet stream (Fig. 5). Yet, there are other factors that can also influence particle transport in the stratosphere. For example, El Nino Southern Oscillation (ENSO) can influence the composition and circulation of the stratosphere in the tropics, by affecting convection-generated waves and the BDC, and in the extratropics, by affecting Rossby waves and pressure systems like the Aleutian Low<sup>75</sup>. Developing a deeper understanding of dynamically driven stratospheric transport variability will be crucial for understanding the time-evolving impacts of a given SAI injection strategy and modifying injections in real-time<sup>76</sup> to continuously optimize SAI's climate impacts, which will be our next step.

Moreover, we want to discuss the uncertainties of this study from three perspectives:

### Injection strategies

Particle transport evaluated in this study can be sensitive to the injection strategies (e.g., injection locations<sup>17,19,20,54</sup>). Previous studies<sup>22,53,77</sup> show that particles injected at higher altitudes tend to have a longer stratospheric lifetime, especially for injection altitudes lower than 21 km. For the same injection altitude, if the injection latitude is closer to the equator, more particles would be transported upwards by the BDC (red vs. blue lines in Fig. 6). Yet, for injections at 19 km (Fig. 6a), most injected particles undergo quasi-horizontal transport: even if we only inject particles at the equator at 19 km (red line in Fig. 6a), fewer than one-third of particles are advected upward by the upwelling flow of BDC. But with injection altitude increasing, more particles tend to transport upward (Fig. 6a vs. Fig. 6b). For injection at 20 km (Fig. 6b), injection at the equator will let more than half of injected particles undergo upward transport (rather than quasi-horizontal transport). In summary, particles injected at higher altitudes or lower latitudes (i.e., closer to the equator) tend to undergo upward transport, while lower-altitude or higher-latitude injections tend to let more particles undergo

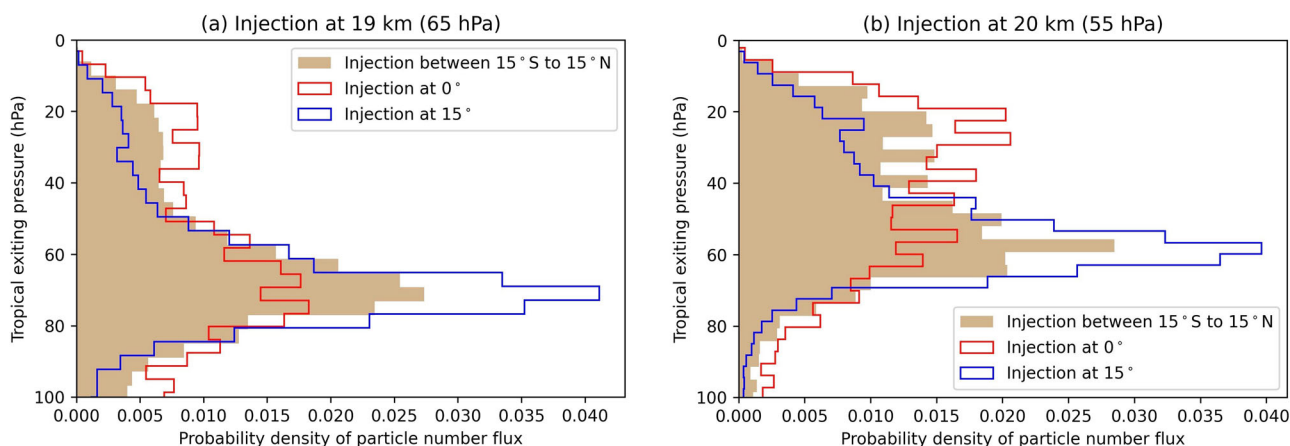


**Fig. 6 | Sensitivity of TM-Flux to injection altitudes and latitudes.** Probability density of TM-Flux (i.e., tropics-to-midlatitude number flux crossing 30° latitude) of particles injected from different altitudes (i.e., a 19 km and b 20 km) and latitudes (0°, 15° S and N, or tropical band between 15° S to 15° N).

quasi-horizontal transport. This is an important consideration for new injection strategies, such as high latitude injection<sup>6,64,78</sup>, which may need further studies regarding particle transport in the stratosphere.

### Lagrangian model (compared to GCMs)

This study uses a Lagrangian method to evaluate particle transport in the stratosphere from a particle-scale perspective. Lagrangian trajectory models, like LAGRANTO in this study, have high computational efficiency and lack of numerical diffusion (compared to GCMs), and by ignoring aerosol microphysics, Lagrangian trajectory models can be efficient tools that allow us to focus on how stratospheric dynamics (e.g., QBO) influence the particle transport. However, because Lagrangian trajectory models mainly represent advective transport, they cannot act like GCMs (which include fully coupled chemical, aerosol, and radiative processes) to fully estimate the climatic impacts of injected particles for SAI. While Lagrangian trajectory models are good at simulating how the background circulation can influence particle transport, it is hard for Lagrangian trajectory models to capture the change of background circulation caused by injected particles. In summary, the Lagrangian trajectory model is useful for research focusing on a specific process, like particle transport in this study. While GCMs can simulate the whole climate system, which is appropriate for fully estimating SAI's climatic impacts. In the future, we will couple a Lagrangian plume model into a global climate model to build a multiscale plume-in-grid model<sup>79</sup>, which includes advantages of both Lagrangian models (e.g., lack of numerical diffusion) and GCMs (e.g., fully coupled chemical, aerosol, and radiative processes).

### Stratospheric transport

This study uses ERA5 data<sup>80</sup>, with 137 vertical levels from 1000 to 0.01 hPa, to offer wind field to drive the LAGRANTO model. Data assimilation in ERA5 data allows a better representation of the stratospheric transport. For example, the COSMIC GNSS-RO dataset assimilated in the ERA5 can provide high-quality temperature information in the upper troposphere and lower/middle stratosphere<sup>81</sup>. However, we have to acknowledge that the representation of the stratospheric circulation in different climate models and reanalysis datasets shows a rather large uncertainty<sup>30,57,82</sup>. For example, results from a Lagrangian CLaMS (Chemical Lagrangian Model of the Stratosphere) model show a significantly slower BDC for ERA5 (compared to ERA-Interim), manifesting in weaker diabatic heating rates and higher age of air<sup>83</sup>. What's more, our model results (driven by reanalysis data) can only represent historical climate. Climate change and other external forcings (e.g., volcano eruptions) in the future can alter the background circulation and particle transport in the stratosphere. Many studies<sup>78,84–86</sup> have found that the radiative effects of injected aerosols from SAI (e.g., stratospheric heating) could meaningfully influence the background circulation. For example, an ECHAM5-HAM model simulation shows that the QBO could slow down and even completely shut down with the increase of sulfate injection due to the radiative heating of injected sulfate aerosols in the stratosphere<sup>46</sup>.

Overall, there are considerable uncertainties regarding injection strategies, modeling methods, and insufficient knowledge of stratospheric transport, which need to be studied in more detail before any technical realization of SAI can be discussed. Lagrangian methods, which can be complementary to GCMs, provide efficient tools for further investigating and constraining these uncertainties.

## Methods

### LAGRANTO model settings

We use the Lagrangian analysis tool LAGRANTO<sup>87</sup>, modified to include sedimentation<sup>33,34</sup>, to track locations of passive particles (without aerosol microphysical growth) injected in the stratosphere based on an SAI injection strategy. In the SAI injection strategy, passive particles are injected once every 3 days at 19 km (65 hPa) within the tropical (from 15° S to 15° N with a 3° interval in latitude, from −180° to 180° with a 15° interval in longitude) stratosphere for 10 years (2000.01–2010.01). The sensitivity of particle transport to two different horizontal injection resolutions is analyzed in the

supporting information (Supplementary Figs. 1 and 2). To emulate particles with a good scattering efficiency, the passive particle is spherical with a radius of 0.2 μm<sup>88,89</sup>, which is smaller than the general effective radius from the SO<sub>2</sub>-injection SAI but close to that from the H<sub>2</sub>SO<sub>4</sub>-injection SAI<sup>59,61,88</sup>. Particle density is the same as the density of sulfate aerosol (1.8 g per cm<sup>3</sup>). 3-hourly ERA5 data<sup>80</sup>, with 1°×1° horizontal resolution and 137 vertical model levels, provides the wind field to drive the LAGRANTO model<sup>29</sup>. Model settings in this study are similar to our previous study<sup>22</sup>, which can be used for further references.

### Calculation of downward stratosphere-to-troposphere particle number flux (ST-flux)

In this study, all particles are initially injected into the tropical lower stratosphere based on a SAI injection strategy. The endpoint of the whole life cycle of injected particles in the stratosphere is when particles cross the tropopause from the stratosphere to the troposphere (i.e., tropospheric sinks of injected particles). This study uses the downward ST-flux, with a unit of particles per km<sup>2</sup> per month (Fig. 5), to represent the tropospheric sink rate. More specifically, if a particle (i) crosses the tropopause from the stratosphere to the troposphere and (ii) stays in the troposphere for more than 3 days, this particle would be considered in the ST-flux calculation. Due to the particle sedimentation and tropospheric wet deposition, the injected particles, which cross the tropopause (considered in the ST-flux calculation), would have less reversible transport (from the troposphere back to the stratosphere) than the massless gases (e.g., air, ozone) in previous studies. Thus, only irreversible downward transport is considered here to define the ST-flux, which meets our research interests in identifying the dominant locations where most particles cross the tropopause from the stratosphere to the troposphere.

### Data availability

The ERA5 data can be accessed from <https://www.ecmwf.int/en/forecasts/dataset/ecmwf-reanalysis-v5>. Tropopause folding (also known as double tropopause) and tropopause height data can be accessed from <https://datapub.fz-juelich.de/slcs/tropopause/>. LAGRANTO model results are openly available from <https://doi.org/10.7910/DVN/UKIBWE>.

### Code availability

Codes for creating the figures and analysis were written in Python and are available from [https://github.com/hongwei8sun/LAGRANTO/tree/main/Python\\_script\\_paper3](https://github.com/hongwei8sun/LAGRANTO/tree/main/Python_script_paper3). Please contact the corresponding author for a latest version.

Received: 30 October 2023; Accepted: 11 May 2024;

Published online: 30 May 2024

## References

1. Wigley, T. M. L. A combined mitigation/geoengineering approach to climate stabilization. *Science* **314**, 452–454 (2006).
2. MacMartin, D. G., Ricke, K. L. & Keith, D. W. Solar geoengineering as part of an overall strategy for meeting the 1.5 °C Paris target. *Philos. Trans. A Math. Phys. Eng. Sci.* **376**, 20160454 (2018).
3. Keith, D. W. Geoengineering the climate: history and prospect. *Annu. Rev. Energy Environ.* **25**, 245–284 (2000).
4. Rasch, P. J. et al. An overview of geoengineering of climate using stratospheric sulphate aerosols. *Philos. Trans. R. Soc. A Math. Phys. Eng. Sci.* **366**, 4007–4037 (2008).
5. Irvine, P. J., Kravitz, B., Lawrence, M. G. & Muri, H. An overview of the Earth system science of solar geoengineering. *Wiley Interdiscip. Rev. Clim. Change* **7**, 815–833 (2016).
6. Visioni, D. et al. Opinion: The scientific and community-building roles of the Geoengineering Model Intercomparison Project (GeoMIP) – past, present, and future. *Atmos. Chem. Phys.* **23**, 5149–5176 (2023).
7. Robock, A. Volcanic eruptions and climate. *Rev. Geophys.* **38**, 191–219 (2000).

8. Vernier, J.-P. et al. Major influence of tropical volcanic eruptions on the stratospheric aerosol layer during the last decade. *Geophys. Res. Lett.* <https://doi.org/10.1029/2011GL047563> (2011).
9. Fuglestedt, H. F., Zhuo, Z., Toohey, M. & Krüger, K. Volcanic forcing of high-latitude Northern Hemisphere eruptions. *npj Clim. Atmos. Sci.* **7**, 10 (2024).
10. Cao, L., Duan, L., Bala, G. & Caldeira, K. Simultaneous stabilization of global temperature and precipitation through cocktail geoengineering. *Geophys. Res. Lett.* **44**, 7429–7437 (2017).
11. Moore, J. C. et al. Atlantic hurricane surge response to geoengineering. *Proc. Natl Acad. Sci. USA* **112**, 13794–13799 (2015).
12. Richter, J. H. et al. Assessing Responses and Impacts of Solar climate intervention on the Earth system with stratospheric aerosol injection (ARISE-SAI): protocol and initial results from the first simulations. *Geosci. Model Dev.* **15**, 8221–8243 (2022).
13. Xia, L., Nowack, P. J., Tilmes, S. & Robock, A. Impacts of stratospheric sulfate geoengineering on tropospheric ozone. *Atmos. Chem. Phys.* **17**, 11913–11928 (2017).
14. Cheng, W. et al. Changes in Hadley circulation and intertropical convergence zone under strategic stratospheric aerosol geoengineering. *npj Clim. Atmos. Sci.* **5**, 32 (2022).
15. Shields, C. A., Richter, J. H., Pendergrass, A. & Tilmes, S. Atmospheric rivers impacting western North America in a world with climate intervention. *npj Clim. Atmos. Sci.* **5**, 41 (2022).
16. Bednarz, E. M., Visioni, D., Richter, J. H., Butler, A. H. & MacMartin, D. G. Impact of the latitude of stratospheric aerosol injection on the southern annular mode. *Geophys. Res. Lett.* **49**, e2022GL100353 (2022).
17. Dai, Z., Weisenstein, D. K. & Keith, D. W. Tailoring meridional and seasonal radiative forcing by sulfate aerosol solar geoengineering. *Geophys. Res. Lett.* **45**, 1030–1039 (2018).
18. Robock, A., Oman, L. & Stenchikov, G. L. Regional climate responses to geoengineering with tropical and Arctic SO<sub>2</sub> injections. *J. Geophys. Res. Atmospheres* <https://doi.org/10.1029/2008JD010050> (2008).
19. Kravitz, B., MacMartin, D. G., Wang, H. & Rasch, P. J. Geoengineering as a design problem. *Earth Syst. Dyn.* **7**, 469–497 (2016).
20. Haywood, J. M., Jones, A., Johnson, B. T. & McFarlane Smith, W. Assessing the consequences of including aerosol absorption in potential stratospheric aerosol injection climate intervention strategies. *Atmos. Chem. Phys.* **22**, 6135–6150 (2022).
21. MacMartin, D. G. et al. The climate response to stratospheric aerosol geoengineering can be tailored using multiple injection locations. *J. Geophys. Res. Atmos.* **122**, 12,574–12,590 (2017).
22. Sun, H., Bourguet, S., Eastham, S. & Keith, D. Optimizing injection locations relaxes altitude-lifetime trade-off for stratospheric aerosol injection. *Geophys. Res. Lett.* **50**, e2023GL105371 (2023).
23. English, J. M., Toon, O. B. & Mills, M. J. Microphysical simulations of sulfur burdens from stratospheric sulfur geoengineering. *Atmos. Chem. Phys.* **12**, 4775–4793 (2012).
24. Yu, F. et al. Particle number concentrations and size distributions in the stratosphere: implications of nucleation mechanisms and particle microphysics. *Atmos. Chem. Phys.* **23**, 1863–1877 (2023).
25. Yu, P. et al. Efficient transport of tropospheric aerosol into the stratosphere via the Asian summer monsoon anticyclone. *Proc. Natl Acad. Sci. USA* **114**, 6972–6977 (2017).
26. Visioni, D., Pitari, G., Tuccella, P. & Curci, G. Sulfur deposition changes under sulfate geoengineering conditions: quasi-biennial oscillation effects on the transport and lifetime of stratospheric aerosols. *Atmos. Chem. Phys.* **18**, 2787–2808 (2018).
27. Konopka, P. et al. Annual cycle of ozone at and above the tropical tropopause: observations versus simulations with the Chemical Lagrangian Model of the Stratosphere (CLaMS). *Atmos. Chem. Phys.* **10**, 121–132 (2010).
28. Hoffmann, L., Rößler, T., Griessbach, S., Heng, Y. & Stein, O. Lagrangian transport simulations of volcanic sulfur dioxide emissions: Impact of meteorological data products. *J. Geophys. Res. Atmos.* **121**, 4651–4673 (2016).
29. Bourguet, S. & Linz, M. The impact of improved spatial and temporal resolution of reanalysis data on Lagrangian studies of the tropical tropopause layer. *Atmos. Chem. Phys.* **22**, 13325–13339 (2022).
30. Charlesworth, E. J., Dugstad, A. K., Fritsch, F., Jöckel, P. & Plöger, F. Impact of Lagrangian transport on lower-stratospheric transport timescales in a climate model. *Atmos. Chem. Phys.* **20**, 15227–15245 (2020).
31. Yin, X. et al. Surface ozone over the Tibetan Plateau controlled by stratospheric intrusion. *Atmos. Chem. Phys.* **23**, 10137–10143 (2023).
32. Yang, J., Wang, K., Lin, M., Yin, X. & Kang, S. Not biomass burning but stratospheric intrusion dominating tropospheric ozone over the Tibetan Plateau. *Proc. Natl Acad. Sci. USA* **119**, e2211002119 (2022).
33. Draxler, R. R. & Hess, G. D. Description of the HYSPLIT\_4 modeling system. NOAA Tech. Memo. ERL ARL-224, 24 (NOAA, 1997).
34. Van der Hoven, I. In *Meteorology and Atomic Energy* (ed. Slade, D. H.) 202–208 (USAEC, 1968).
35. Torrence, C. & Compo, G. P. A practical guide to wavelet analysis. *Bull. Am. Meteorol. Soc.* **79**, 61–78 (1998).
36. Liu, Y., San Liang, X. & Weisberg, R. H. Rectification of the bias in the wavelet power spectrum. *J. Atmos. Ocean Technol.* **24**, 2093–2102 (2007).
37. Baldwin, M. P. et al. The quasi-biennial oscillation. *Rev. Geophys.* **39**, 179–229 (2001).
38. Hsu, J. & Prather, M. J. Stratospheric variability and tropospheric ozone. *J. Geophys. Res. Atmos.* <https://doi.org/10.1029/2008JD010942> (2009).
39. Wang, M., Fu, Q., Hall, A. & Sweeney, A. Stratosphere-troposphere exchanges of air mass and ozone concentrations from ERA5 and MERRA2: Annual-mean climatology, seasonal cycle, and interannual variability. *J. Geophys. Res. Atmos.* **128**, e2023JD039270 (2023).
40. Plumb, R. A. & Bell, R. C. A model of the quasi-biennial oscillation on an equatorial beta-plane. *Q. J. R. Meteorol. Soc.* **108**, 335–352 (1982).
41. Punge, H. J., Konopka, P., Giorgetta, M. A. & Müller, R. Effects of the quasi-biennial oscillation on low-latitude transport in the stratosphere derived from trajectory calculations. *J. Geophys. Res. Atmos.* <https://doi.org/10.1029/2008JD010518> (2009).
42. Holton, J. R. & Tan, H.-C. The influence of the equatorial quasi-biennial oscillation on the global circulation at 50 mb. *J. Atmos. Sci.* **37**, 2200–2208 (1980).
43. Baldwin, M. P. & Dunkerton, T. J. Quasi-biennial modulation of the southern hemisphere stratospheric polar vortex. *Geophys. Res. Lett.* **25**, 3343–3346 (1998).
44. Garfinkel, C. I., Shaw, T. A., Hartmann, D. L. & Waugh, D. W. Does the Holton–Tan mechanism explain how the quasi-biennial oscillation modulates the Arctic polar vortex? *J. Geophys. Res. Atmos.* **69**, 1713–1733 (2012).
45. Flury, T., Wu, D. L. & Read, W. G. Variability in the speed of the Brewer–Dobson circulation as observed by Aura/MLS. *Atmos. Chem. Phys.* **13**, 4563–4575 (2013).
46. Niemeier, U. & Schmidt, H. Changing transport processes in the stratosphere by radiative heating of sulfate aerosols. *Atmos. Chem. Phys.* **17**, 14871–14886 (2017).
47. Hoffmann, L. & Spang, R. An assessment of tropopause characteristics of the ERA5 and ERA-Interim meteorological reanalyses. *Atmos. Chem. Phys.* **22**, 4019–4046 (2022).
48. Garfinkel, C. I. & Hartmann, D. L. The influence of the quasi-biennial oscillation on the troposphere in winter in a hierarchy of models. Part II: perpetual winter WACCM runs. *J. Atmos. Sci.* **68**, 2026–2041 (2011).
49. Haynes, P. et al. The influence of the stratosphere on the tropical troposphere. *J. Meteorol. Soc. Jpn. Ser. II* **99**, 803–845 (2021).
50. Silverman, V., Lubis, S. W., Harnik, N. & Matthes, K. A synoptic view of the onset of the midlatitude QBO signal. *J. Atmos. Sci.* **78**, 3759–3780 (2021).

51. Kumar, V., Yoden, S. & Hitchman, M. H. QBO and ENSO effects on the mean meridional circulation, polar vortex, subtropical westerly jets, and wave patterns during boreal winter. *J. Geophys. Res. Atmos.* **127**, e2022JD036691 (2022).
52. Gray, L. J. et al. Surface impacts of the quasi biennial oscillation. *Atmos. Chem. Phys.* **18**, 8227–8247 (2018).
53. Tilmes, S. et al. Sensitivity of aerosol distribution and climate response to stratospheric SO<sub>2</sub> injection locations. *J. Geophys. Res. Atmos.* **122**, 12,591–12,615 (2017).
54. Visioni, D. et al. Climate response to off-equatorial stratospheric sulfur injections in three Earth system models – Part 1: experimental protocols and surface changes. *Atmos. Chem. Phys.* **23**, 663–685 (2023).
55. Lin, P. & Fu, Q. Changes in various branches of the Brewer–Dobson circulation from an ensemble of chemistry climate models. *J. Geophys. Res. Atmos.* **118**, 73–84 (2013).
56. Hall, T. M. & Plumb, R. A. Age as a diagnostic of stratospheric transport. *J. Geophys. Res. Atmos.* **99**, 1059–1070 (1994).
57. Linz, M. et al. The strength of the meridional overturning circulation of the stratosphere. *Nat. Geosci.* **10**, 663–667 (2017).
58. WMO. WMO Meteorology - a three-dimensional science. Second session of the commission for aerology. *WMO Bull.* **IV**, 134–138 (1957).
59. Vattioni, S. et al. Exploring accumulation-mode H<sub>2</sub>SO<sub>4</sub> versus SO<sub>2</sub> stratospheric sulfate geoengineering in a sectional aerosol–chemistry–climate model. *Atmos. Chem. Phys.* **19**, 4877–4897 (2019).
60. Lee, W., MacMartin, D., Visioni, D. & Kravitz, B. Expanding the design space of stratospheric aerosol geoengineering to include precipitation-based objectives and explore trade-offs. *Earth Syst. Dyn.* **11**, 1051–1072 (2020).
61. Weisenstein, D. K. et al. An interactive stratospheric aerosol model intercomparison of solar geoengineering by stratospheric injection of SO<sub>2</sub> or accumulation-mode sulfuric acid aerosols. *Atmos. Chem. Phys.* **22**, 2955–2973 (2022).
62. Kravitz, B., Robock, A., Oman, L., Stenchikov, G. & Marquardt, A. B. Sulfuric acid deposition from stratospheric geoengineering with sulfate aerosols. *J. Geophys. Res. Atmos.* <https://doi.org/10.1029/2009jd011918> (2009).
63. Visioni, D. et al. What goes up must come down: impacts of deposition in a sulfate geoengineering scenario. *Environ. Res. Lett.* **15**, 094063 (2020).
64. Lee, W. R. et al. High-latitude stratospheric aerosol injection to preserve the Arctic. *Earth's Future* **11**, e2022EF003052 (2023).
65. Visioni, D., Pitari, G., di Genova, G., Tilmes, S. & Cionni, I. Upper tropospheric ice sensitivity to sulfate geoengineering. *Atmos. Chem. Phys.* **18**, 14867–14887 (2018).
66. Sporre, M. K., Friberg, J., Svenhag, C., Sourdeval, O. & Storelvmo, T. Springtime stratospheric volcanic aerosol impact on midlatitude cirrus clouds. *Geophys. Res. Lett.* **49**, e2021GL096171 (2022).
67. Eastham, S. D., Weisenstein, D. K., Keith, D. W. & Barrett, S. R. H. Quantifying the impact of sulfate geoengineering on mortality from air quality and UV-B exposure. *Atmos. Environ.* **187**, 424–434 (2018).
68. Seo, K.-H. & Bowman, K. P. Lagrangian estimate of global stratosphere–troposphere mass exchange. *J. Geophys. Res. Atmos.* **107**, ACL 2-1–ACL 2-8 (2002).
69. Škerlak, B., Sprenger, M., Pfahl, S., Tyrlis, E. & Wernli, H. Tropopause folds in ERA-Interim: global climatology and relation to extreme weather events. *J. Geophys. Res. Atmos.* **120**, 4860–4877 (2015).
70. Stohl, A. et al. Stratosphere–troposphere exchange: a review, and what we have learned from STACCATO. *J. Geophys. Res. Atmos.* <https://doi.org/10.1029/2002jd002490> (2003).
71. Stohl, A. et al. A new perspective of stratosphere–troposphere exchange. *Bull. Am. Meteorol. Soc.* **84**, 1565–1574 (2003).
72. Gettelman, A. et al. The extratropical upper troposphere and lower stratosphere. *Rev. Geophys.* <https://doi.org/10.1029/2011RG000355> (2011).
73. Škerlak, B., Sprenger, M. & Wernli, H. A global climatology of stratosphere–troposphere exchange using the ERA-Interim data set from 1979 to 2011. *Atmos. Chem. Phys.* **14**, 913–937 (2014).
74. Boothe, A. C. & Homeyer, C. R. Global large-scale stratosphere–troposphere exchange in modern reanalyses. *Atmos. Chem. Phys.* **17**, 5537–5559 (2017).
75. Domeisen, D. I. V., Garfinkel, C. I. & Butler, A. H. The teleconnection of El Niño southern oscillation to the stratosphere. *Rev. Geophys.* **57**, 5–47 (2019).
76. Aksamit, N. O., Kravitz, B., MacMartin, D. G. & Haller, G. Harnessing stratospheric diffusion barriers for enhanced climate geoengineering. *Atmos. Chem. Phys.* **21**, 8845–8861 (2021).
77. Lee, W. R. et al. Quantifying the efficiency of stratospheric aerosol geoengineering at different altitudes. *Geophys. Res. Lett.* **50**, e2023GL104417 (2023).
78. Bednarz, E. M. et al. Climate response to off-equatorial stratospheric sulfur injections in three Earth system models – Part 2: stratospheric and free-tropospheric response. *Atmos. Chem. Phys.* **23**, 687–709 (2023).
79. Sun, H., Eastham, S. & Keith, D. Developing a plume-in-grid model for plume evolution in the stratosphere. *J. Adv. Model. Earth Syst.* **14**, e2021MS002816 (2022).
80. Hersbach, H. et al. The ERA5 global reanalysis. *Q. J. R. Meteorol. Soc.* **146**, 1999–2049 (2020).
81. Long, C. S., Fujiwara, M., Davis, S., Mitchell, D. M. & Wright, C. J. Climatology and interannual variability of dynamic variables in multiple reanalyses evaluated by the SPARC Reanalysis Intercomparison Project (S-RIP). *Atmos. Chem. Phys.* **17**, 14593–14629 (2017).
82. Ploeger, F. et al. How robust are stratospheric age of air trends from different reanalyses? *Atmos. Chem. Phys.* **19**, 6085–6105 (2019).
83. Ploeger, F. et al. The stratospheric Brewer–Dobson circulation inferred from age of air in the ERA5 reanalysis. *Atmos. Chem. Phys.* **21**, 8393–8412 (2021).
84. Heckendorn, P. et al. The impact of geoengineering aerosols on stratospheric temperature and ozone. *Environ. Res. Lett.* **4**, 045108 (2009).
85. Richter, J. H. et al. Stratospheric dynamical response and ozone feedbacks in the presence of SO<sub>2</sub> injections. *J. Geophys. Res. Atmos.* **122**, 12,557–12,573 (2017).
86. Karami, K., Garcia, R., Jacobi, C., Richter, J. H. & Tilmes, S. The Holton–Tan mechanism under stratospheric aerosol intervention. *Atmos. Chem. Phys.* **23**, 3799–3818 (2023).
87. Sprenger, M. & Wernli, H. The LAGRANTO Lagrangian analysis tool – version 2.0. *Geosci. Model Dev.* **8**, 2569–2586 (2015).
88. Pierce, J. R., Weisenstein, D. K., Heckendorn, P., Peter, T. & Keith, D. W. Efficient formation of stratospheric aerosol for climate engineering by emission of condensable vapor from aircraft. *Geophys. Res. Lett.* <https://doi.org/10.1029/2010GL043975> (2010).
89. Dykema, J. A., Keith, D. W. & Keutsch, F. N. Improved aerosol radiative properties as a foundation for solar geoengineering risk assessment. *Geophys. Res. Lett.* **43**, 7758–7766 (2016).

## Acknowledgements

This work was funded by the Solar Geoengineering Research Program at Harvard University and the Climate Systems Engineering Initiative at the University of Chicago. We thank Qiang Fu and Mingcheng Wang from the University of Washington for the discussion of stratospheric dynamics. The computations in this study were run on the FASRC Cannon cluster at Harvard University.

## Author contributions

H.S.: conceptualization, data curation, formal analysis, investigation, methodology, writing the original draft, editing. S.B.: discussion of results,



methodology, investigation, editing. L.L.: discussion of results, investigation, editing. D.K.: discussion of results, editing, funding acquisition.

### Competing interests

The authors declare no competing interests.

### Additional information

**Supplementary information** The online version contains supplementary material available at

<https://doi.org/10.1038/s41612-024-00664-8>.

**Correspondence** and requests for materials should be addressed to Hongwei Sun.

**Reprints and permissions information** is available at <http://www.nature.com/reprints>

**Publisher's note** Springer Nature remains neutral with regard to jurisdictional claims in published maps and institutional affiliations.

**Open Access** This article is licensed under a Creative Commons Attribution 4.0 International License, which permits use, sharing, adaptation, distribution and reproduction in any medium or format, as long as you give appropriate credit to the original author(s) and the source, provide a link to the Creative Commons licence, and indicate if changes were made. The images or other third party material in this article are included in the article's Creative Commons licence, unless indicated otherwise in a credit line to the material. If material is not included in the article's Creative Commons licence and your intended use is not permitted by statutory regulation or exceeds the permitted use, you will need to obtain permission directly from the copyright holder. To view a copy of this licence, visit <http://creativecommons.org/licenses/by/4.0/>.

© The Author(s) 2024